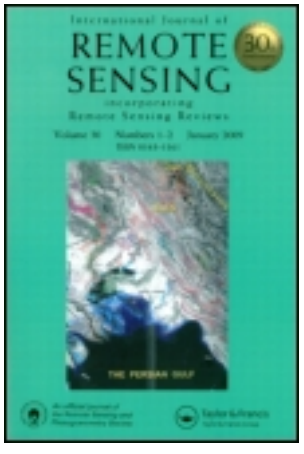

International Journal of Remote Sensing

Publication details, including instructions for authors and subscription information:
http://www.tandfonline.com/loi/tres20

Convective cloud discrimination using multi-frequency microwave signatures of the AMSR-E sensor: evaluation over the Tibetan Plateau

David Kuria [a] & Toshio Koike [b]

[a] Department of Geomatic Engineering and Geospatial Information Systems, Jomo Kenyatta University of Agriculture and Technology, P.O. Box 62000-00200, Nairobi, Kenya

[b] Department of Civil Engineering, River and Environmental Engineering Laboratory, University of Tokyo, Tokyo, 113-8656, Japan

Available online: 28 Jun 2011

To cite this article: David Kuria & Toshio Koike (2011): Convective cloud discrimination using multi-frequency microwave signatures of the AMSR-E sensor: evaluation over the Tibetan Plateau, International Journal of Remote Sensing, 32:12, 3451-3460

To link to this article: http://dx.doi.org/10.1080/01431161003749451

International Journal of Remote Sensing
Vol. 32, No. 12, 20 June 2011, 3451–3460

Taylor & Francis
Taylor & Francis Group

Convective cloud discrimination using multi-frequency microwave signatures of the AMSR-E sensor: evaluation over the Tibetan Plateau

DAVID KURIA*† and TOSHIO KOIKE‡
†Department of Geomatic Engineering and Geospatial Information Systems, Jomo Kenyatta University of Agriculture and Technology, P.O. Box 62000-00200, Nairobi, Kenya
‡Department of Civil Engineering, River and Environmental Engineering Laboratory, University of Tokyo, Tokyo 113-8656, Japan

(*Received 29 December 2008; in final form 27 January 2010*)

Multi-frequency passive microwave remote sensing affords a unique opportunity to understand various phenomena; low-frequency microwaves penetrate clouds and are able to observe Earth surface conditions (~6–18 GHz), while the higher frequencies are strongly impacted by prevailing atmospheric conditions. By using these relationships, an atmospheric opacity index (AOI) using Advanced Microwave Scanning Radiometer on Earth Observing Satellite (AMSR-E) multi-frequency data is proposed. This index utilizes four AMSR-E frequencies spanning both high- and low-microwave frequency. This AOI can be used to discriminate cloudy atmosphere from clear-sky conditions.

This index shows good agreement with current cloud indices. In this research, it is compared against the Moderate Imaging Spectroradiometer (MODIS) and the Geostationary Operational Environmental Satellite 9th series (GOES-9) atmosphere products. It offers the possibility of detecting convective clouds at all times (day and night) due to the advantage of the independence of the microwave sensors on the Sun for illumination.

1. Introduction

Cloud information is used to predict weather, from extreme weather events to normal weather conditions (Horvath and Davies 2001). While an array of satellites used for weather prediction and climate research have been deployed in space, such as the Geostationary Operational Environmental Satellite (GOES) utilizing visible and infrared bands, other non-weather sensors such as the Tropical Rainfall Monitoring Mission (TRMM) and the Advanced Microwave Spectroradiometer on the Earth Observing Mission (AMSR-E) operating at microwave frequencies, have the potential to add value to weather-deduced information from weather satellites.

To make use of satellite data in obtaining estimates of surface variables, it is often necessary to use cloud-free data. One of the early approaches to obtain cloud information was using data from the Advanced Very High Resolution Radiometer (AVHRR) by Saunders and Kriebel (1988). They developed a cloud-analysis scheme using AVHRR data for obtaining both surface and cloud parameters in near real

*Corresponding author. Email: dn.kuria@gmail.com

International Journal of Remote Sensing
ISSN 0143-1161 print/ISSN 1366-5901 online
http://www.tandf.co.uk/journals
DOI: 10.1080/01431161003749451

time. This scheme used information on all five channels of the AVHRR. It used five tests for detecting and identifying pixels as cloud free.

Recently, Jedlovec and Laws (2003) developed a bi-spectral threshold (BTH) method for detecting clouds under low Sun angles using GOES data. Compared with the bi-spectral spatial coherence (BSC) method, the BTH approach was reported as giving significantly improved cloud-detection capabilities. The Moderate Imaging Spectroradiometer (MODIS) cloud-temperature data have been used to infer presence of clouds, as observed low cloud temperatures are interpreted as an indication of cloud presence (Fujii and Koike 2001).

Passive microwave space-borne sensors are able to overcome the limitations of the dependency of the optical sensors on solar illumination (Ulaby *et al.* 1981, Lillesand *et al.* 2004). Moreover, current trends in sensor launches have been heavily biased towards multi-spectral, hyper-spectral or multi-channel (Kummerow *et al.* 2001). These provide a unique opportunity to study both atmosphere and land-surface conditions by utilizing the spectral-response patterns of targets. This trend gave impetus to this research activity, as it sought to identify an all-weather strategy for discriminating cloud coverage. Pfaff (2003) evaluated and refined the four-stream radiative-transfer model developed by Liu (1998) using AMSR-E and Ground Based Microwave Radiometer (GBMR) data over Wakasa Bay in Japan. Liu showed that the model could simulate snowfall over this bay. Furthermore, Mirza (2005) developed an ice microphysics data-assimilation scheme that assimilated AMSR-E brightness temperature over Wakasa Bay. In this scheme, it was possible to retrieve integrated cloud liquid water and integrated water-vapour content. These approaches worked well over extensive water bodies such as oceans, lakes and seas, and are reported to fail when applied over land due to the change in the boundary conditions.

A comparison of retrieval skill using AMSR-E and MODIS datasets was given by Juarez *et al.* (2009). They observed that liquid–water path (LWP) retrievals are very similar in overcast conditions for both sensors.

The objective of this research was thus to identify and propose a means through which cloud cover (convective systems) can be identified from passive microwave imageries. To accomplish this, time series AMSR-E imageries were obtained from the Coordinated Enhanced Observing Period (CEOP) project. The CEOP project has excellent long-term datasets that can be used for improving understanding on the global hydrologic cycle. In this research, the CEOP Tibet site was selected since it has a complete dataset: imageries, *in situ* data and weather-forecast model simulation results.

2. The Tibet CEOP site

Figure 1 shows the CEOP site. The Tibetan Plateau is 4000 m above sea level, 3000 km long in longitude and 1000 km wide in latitude. It experiences strong surface solar radiation, and has low pressure and low air density, but a wide range of air temperatures. It experiences strong diurnal and seasonal variation of land cover, energy partition, cloud cover and rainfall. During the monsoon season, it experiences a lot of rainfall, but there is a big contrast in rainfall and land cover between the eastern and western parts of the plateau (Yang *et al.* 2005). The plateau surfaces are typically characterized by alpine meadows and grasslands in the central and eastern parts, while the western part is dominated by alpine deserts (Yang *et al.* 2009). Due to this variability, it was selected by the CEOP project to assist in studying climatic and hydrologic phenomena in eastern Asia.

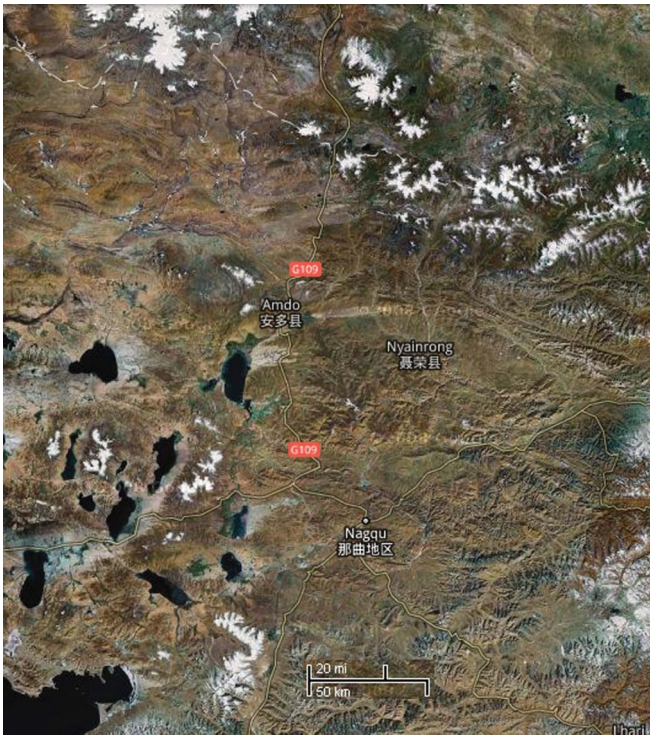

Figure 1. The CEOP Tibet site. The red pegs mark the extents corresponding to the AMSR-E image. The four *in situ* stations are marked with small yellow pegs. This image was obtained from Google Earth™. © 2008 Google; Mapdata © 2008 Mapabc; Image © 2008 GeoEye; Image © 2008 Terrametrics.

An array of data is available for this site; however, direct cloud observations, which can be inferred from satellite imageries, are lacking. On some days, there were nearly coincident MODIS, GOES-9 and AMSR-E satellite observations, which were archived for the site. These data were obtained by using the CEOP project data client developed by Nemoto *et al.* (2007).

The data for each of the 12 AMSR-E channels were resampled using the cubic-convolution method to a resolution of 0.05° (~5 km), corresponding to the spatial resolution of the 89 GHz data. This resolution was chosen since the data at the higher frequencies show greater variability, while bearing in mind the limitation of data availability. Other researchers have shown satisfactory results utilizing resampled resolutions of 0.1° (~10 km) with similar datasets at lower frequencies (Yang *et al.* 2007), from which they were able to obtain good distributions of soil moisture.

2.1 *Cloud observations*

Datasets for the periods of April and August 2004 were used. These correspond to the end of winter and midsummer, respectively. During the winter period, there is significant snow coverage, while in summertime, heavy rain events do occur (Yang *et al.* 2005). For illustration purposes, data collected on 20 August 2004 during which a precipitation event was recorded on the site is considered.

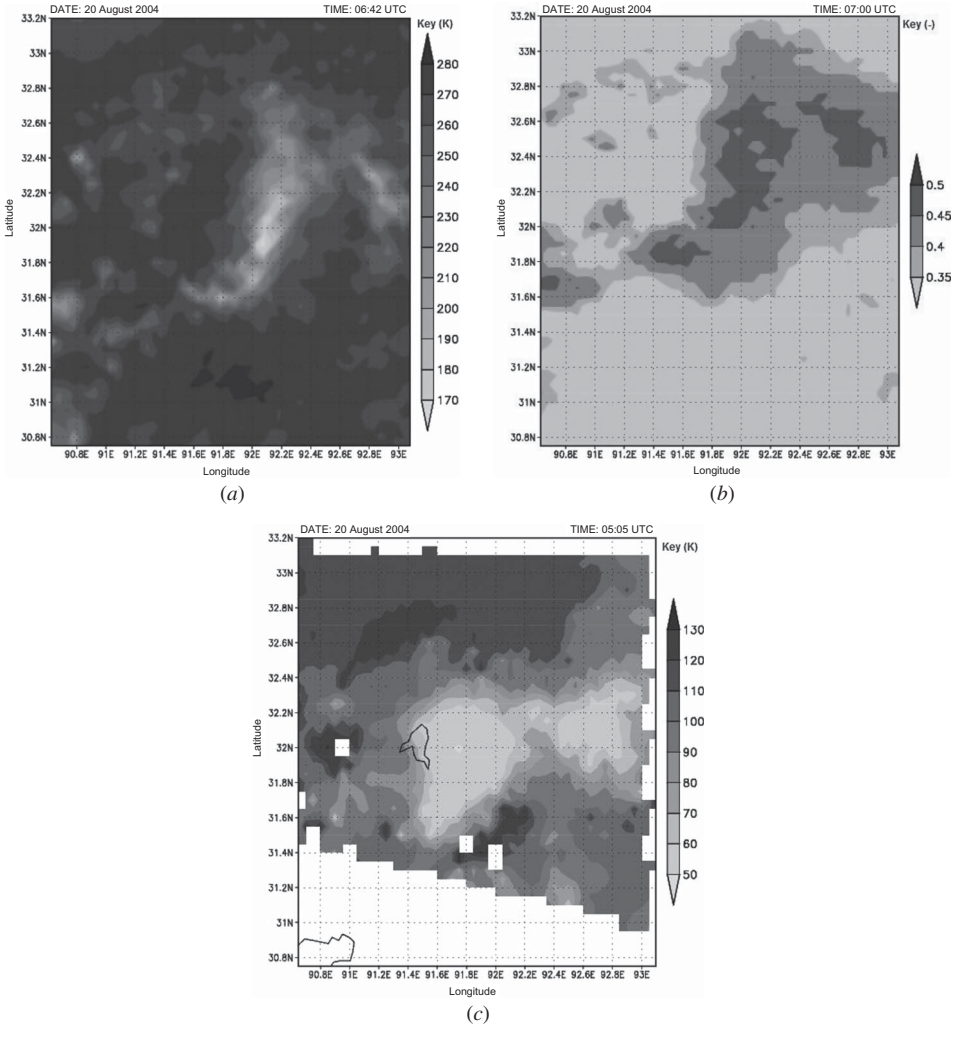

Figure 2. Satellite observations for 20 August 2004. (*a*) AMSR-E observed 89 GHz vertical polarized brightness temperatures obtained at 06:42 UTC. (*b*) GOES-9 cloud-albedo map obtained at 07:00 UTC and (*c*) MODIS cloud-top temperatures obtained at 05:05 UTC.

From the AMSR-E image taken on this day (figure 2(*a*)), it is suspected that there was a heavy cloud presence and possibly a precipitation event on the site during the AMSR-E overpass time at 06:42 UTC due to very cold brightness temperatures recorded during this overpass time. This phenomenon could be due to the presence of convective clouds and perhaps precipitating clouds.

To justify this hypothesis and to serve as an appropriate illustration, figure 2(*a*) is compared with the observed cloud albedo from the GOES-9 satellite (figure 2(*b*)) at 07:00 UTC, and the MODIS cloud-top temperature (figure 2(*c*)) at 05:05 UTC. Considering the respective observation times, it can be observed that the GOES-9 albedo map shows better agreement with the brightness-temperature map. The cloud structure in the GOES image agrees well with the brightness-temperature map, even though it was obtained 18 minutes after the AMSR-E observation. From

the MODIS cloud-top temperature, it can be seen that 1.5 hours earlier, there was a heavy cloud presence at the site.

From the GOES-9 albedo image, the type of cloud cover is probably the cumulus-nimbus type (opaque), typical for this site (Iguchi *et al.* 2002), and is normally accompanied by heavy precipitation. In the very cold region (corresponding to 170–200 K brightness temperatures in the AMSR-E image), there is a likelihood of large hydrometeors in both liquid and frozen forms, which significantly attenuate surface and atmospheric emission by absorption and scattering (Ulaby *et al.* 1986), leading to very low brightness-temperature observations.

2.2 *GOES albedo*

The visible (VIS) channel GOES radiances are calibrated against the visible channels of the National Oceanic and Atmospheric Administration (NOAA) Advanced Very High Resolution Radiometer (AVHRR) (Doelling *et al.* 1998). The calibration of GOES VIS data is described in Ayers *et al.* (1998). For most applications, the VIS radiances (L) are converted to VIS albedo (α_n) according to

$$\alpha_n = \frac{\pi}{L}\delta(d)\mu_0 E\chi(\mu_0, \mu, \psi), \tag{1}$$

where δ is the Earth–Sun-distance correction factor for Julian day d, E is the VIS solar constant for GOES, $E = 526.9\ \mathrm{W\ m^{-2}\ sr^{-1}\ \mu m^{-1}}$, μ_0 and μ are the cosines of the viewing and solar zenith angles respectively, ψ is the relative azimuth angle and χ is the bi-directional-reflectance model described by Minnis and Harrison (1984). The bi-directional model depends on the scene with distinct values for three surface types: clear water, land and clouds. If a scene is mixed, albedos are calculated for each surface type, then averaged according to the weight of each surface type.

This GOES albedo product has been used in many research activities as an aid for retrieval of other variables such as in clear-sky-temperature estimation and land-surface fluxes (Khaiyer *et al.* 2002). A detailed description of the algorithms used in computing the albedo is given in Doelling *et al.* (1998) and references cited therein.

3. The atmosphere opacity index

Electromagnetic radiation interacts with targets in different, but comparable, fashion depending on particle sizes, surface conditions, water content and the wavelength of the radiation (Ulaby *et al.* 1981, Jensen 2000, Lillesand *et al.* 2004). As it has multi-channel sensors, the AMSR-E offers a unique promise by utilizing the data at the various channels in a unified way. After testing various possible indices utilizing various combinations of vertical polarization and horizontal polarization for the channel sets (6, 10 36, 89), (10, 18, 36, 89), (10, 23, 36, 89) and (6, 23, 36, 89), it was found that the combination utilizing vertically polarized channels (10, 23, 36, 89) gave the best agreement with existing cloud metrics. This relationship is presented formally in equation (2), and can be used to identify possible cloud-covered pixels:

$$\mathrm{AOI} = -\frac{T_{B_{89v}} - T_{B_{36v}}}{T_{B_{89v}} + T_{B_{36v}}} \Big/ \frac{T_{B_{23v}} - T_{B_{10v}}}{T_{B_{23v}} + T_{B_{10v}}}, \tag{2}$$

where AOI refers to the atmosphere opacity index, T_B is the brightness temperature and the subscripts 10, 23, 36 and 89 refer to the frequencies in GHz and v to vertical polarization. Figure 3 shows atmosphere opacity (AO) maps compared with the

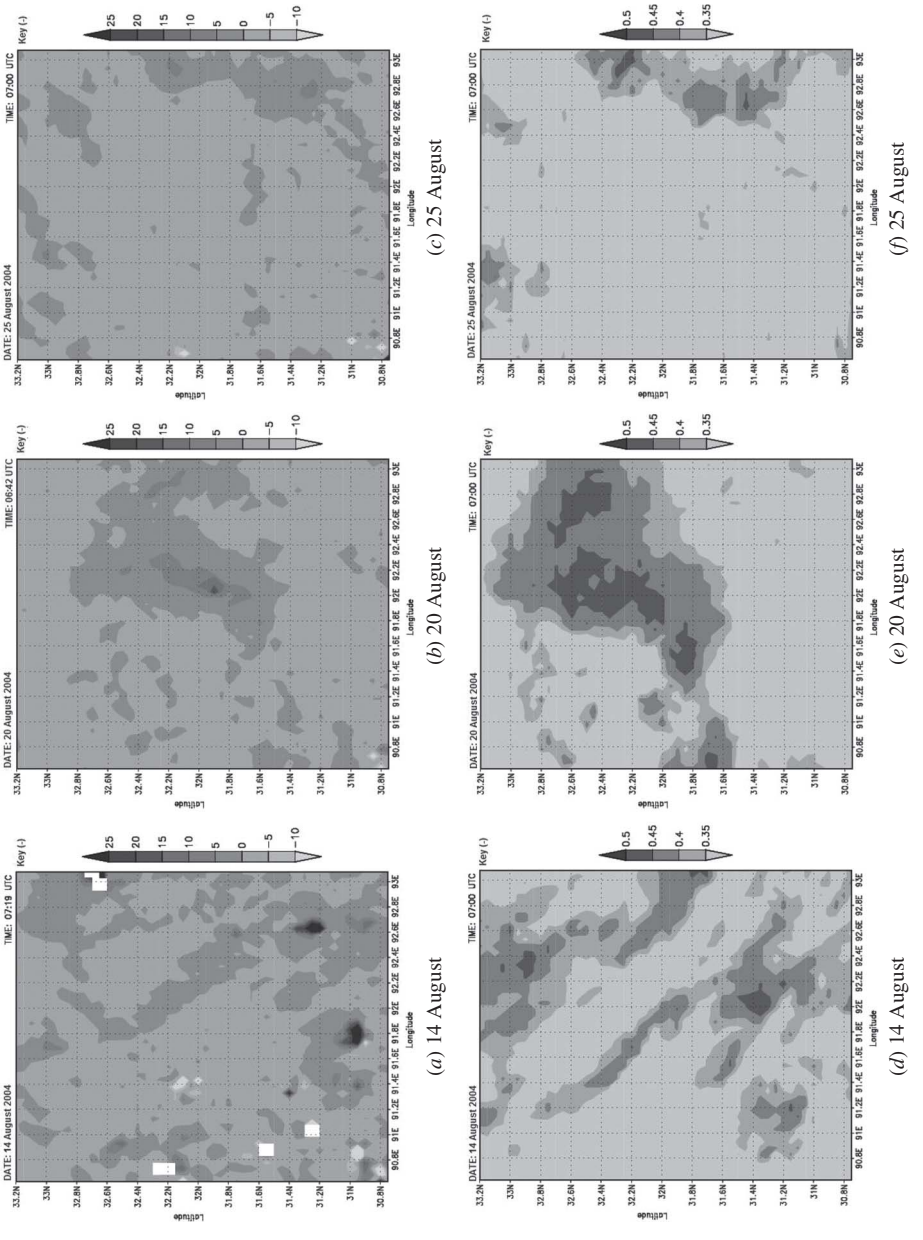

(*a*) 14 August (*b*) 20 August (*c*) 25 August

(*d*) 14 August (*e*) 20 August (*f*) 25 August

Figure 3. Comparison between (*a*)–(*c*) atmosphere opacity indices and (*d*)–(*f*) corresponding cloud albedo for days with nearly coincident observation instances and with significant cloud cover.

GOES-9 cloud albedo. These AO maps were obtained by calculating an AOI for each grid point using equation (2), which relates 18.7, 23.8, 36.5 and 89 GHz vertically polarized observed brightness temperatures. This index was inspired by work undertaken by Paloscia and Pampaloni (1988) and Fujii and Koike (2001), who proposed indices for discriminating soil moisture using lower frequency microwaves.

These AO maps show remarkable agreement with the GOES-9 albedo images. For the entire period of August, reasonable agreement between the proposed index and the GOES albedo product was found as represented by figure 3. The three days shown here had significant cloud cover and were observed at nearly coincident times ($< |20|$ minutes). There is nearly complete visual agreement between these two image sets. This research considered only the ascending overpass data from AMSR-E since GOES albedo data are only available during the day. It is therefore proposed that this index can be used to obtain opacity estimates of the atmosphere when it is not feasible to use the visible band, for example, at night, or when supplementary cloud information is lacking or unreliable. Cloud cover can be deduced from the following condition:

$$\text{cloud cover} = \begin{cases} \text{AOI} > 5, & \text{cloudy}, \\ \text{otherwise}, & \text{clearsky}. \end{cases} \tag{3}$$

The threshold in this equation was arrived at after comparison with corresponding thresholds from the GOES albedo product ($\sim$0.33). The AOI has some nice features since it is able to remove or minimize not only temperature dependence, but also the effects of land-surface heterogeneity. The area surrounding the water surfaces (identifiable in figure 1), are not identifiable in these cases, implying that the effect of surface-type dependence has been suppressed.

While a direct correspondence between the GOES albedo and the AMSR-E AOI was difficult to accomplish due to the different observation times for the two sensors, a scatterplot of data from these two products was prepared (figure 4). This figure shows a direct correlation between the albedo and the AOI. From this index, a qualitative assessment of cloud cover can be obtained. This can be used when

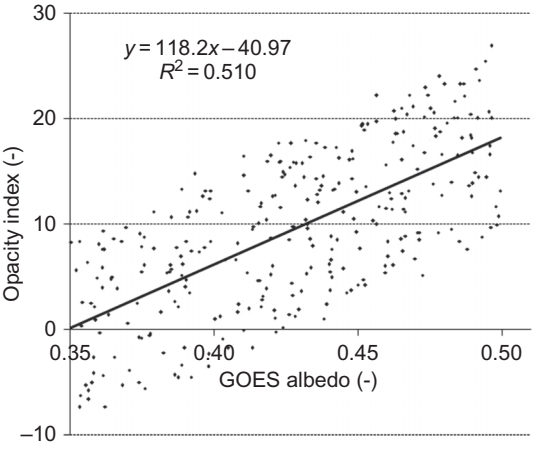

Figure 4. Scatterplot for a sample of 600 pixels showing correspondence between AMSR-E AOI and GOES albedo values.

preliminary discrimation of cloud-covered pixels is desired to facilitate further analysis of the images, irrespective of time of day.

3.1 *Physical meaning of the AOI*

At low microwave frequencies, the atmosphere is transparent, hence observations at 10.65 GHz can be assumed to contain no information about atmosphere, but capture the information about the ground-surface conditions. The frequency 23.8 GHz is very sensitive to the water-vapour condition of the atmosphere and prevailing ground conditions. Thus, the relationship $(T_{B_{23v}} - T_{B_{10v}})/(T_{B_{23v}} + T_{B_{10v}})$ 'normalizes' 23.8 GHz data by minimizing the contribution from land-surface conditions, while enhancing the contribution from the atmosphere. This line of argument follows the normalized difference vegetation index (NDVI) (Lillesand *et al.* 2004). Mirza (2005) demonstrated that using AMSR-E brightness-temperature data (23.7 and 35 GHz), it is possible to obtain integrated water-vapour content.

Fujii and Koike (2001) developed an index utilizing 6.925, 18.7 and 85 GHz horizontally polarized channels on the Tropical Rainfall Measuring Mission (TRMM) Microwave Imager (TMI) to obtain soil wetness and estimates of precipitation over the Tibetan Plateau. From their work, there is potential to retrieve atmospheric variables using these frequencies, in addition to surface variables. Since AMSR-E frequencies lie very close to those of the TMI, these findings can also be extended to it.

Higher microwave frequencies are more sensitive to atmosphere conditions, and thus both 36.5 and 89 GHz observations contain substantial information about atmosphere. The 89 GHz observations are impacted more strongly by atmosphere conditions than the 36.5 GHz observations. The relationship $(T_{B_{89v}} - T_{B_{36v}})/(T_{B_{89v}} + T_{B_{36v}})$ therefore, enhances the signature from the atmosphere. While both these frequencies capture significant information about the atmosphere, this information is limited to conditions related to convective activities. Most of the research conducted on retrieval of cloud ice, cloud liquid and water vapour has been limited to using frequencies in the ranges 20–24, 34–36 and 85–90 GHz (Liou and Duff 1979, Li *et al.* 1997, Vivekanandan *et al.* 1997). For non-convective systems such as cirrus clouds, frequencies higher than those used in this research are appropriate (Ulaby *et al.* 1986).

The proposed index, AOI, is thus a combination of 'enhanced' atmosphere conditions (signatures) from higher microwave frequencies and the 'normalized' land-surface conditions from the lower microwave frequencies. This index masks out the effect of the land surface, capturing the prevailing convective situation of the atmosphere.

4. Conclusion

In this article, an AOI has been proposed. Time-series data for the month of August 2004 AMSR-E brightness temperatures were investigated with a view to identifying overpasses in which convective clouds were present . There were few corresponding GOES-9 albedo and MODIS cloud-top temperature data available for comparison with the proposed index. This AOI has been demonstrated as having a direct correlation with GOES-9 cloud albedo maps, which were obtained using visible channels of the GOES sensor.

AMSR-E satellite data at 06:42 UTC on 20 August 2004 were investigated when studying the possibilities of obtaining cloud information from the AMSR-E sensor.

It was found that, on this date, very low brightness-temperature values were recorded, whose distribution compared very well with GOES-9 albedo and MODIS cloud-top temperature products. Thus, these low brightness-temperature values pointed to a high likelihood of convective cloud cover in the region at the AMSR-E overpass time. This observation inspired the proposition of the AOI. Several indices were investigated, but the best results were obtained by using equation (2). This AOI was developed by employing vertically polarized brightness temperatures at 10.65, 23.7, 36.5 and 89 GHz data.

This index was compared with nearly coincident GOES-9 albedo images and showed good visual agreement. A scatterplot of the relationship between AOI and albedo has shown that, despite the overpass times for the two sensors being different, there is a direct correlation between the two, and thus one can be used to augment the other. This quantitative evaluation of AOI shows the potential that the index has with respect to identifying cloud-covered pixels, irrespective of the time of day.

By utilizing the AOI, it has been shown that it is possible to obtain convective cloud-coverage information. This index can be used in all weather conditions, unlike the GOES-9 albedo product, which can only be obtained during the day when there is sufficient sunlight.

Acknowledgements

The authors wish to acknowledge the critical input of the two peer reviewers who helped to improve the overall scholarly content of this work. This research was supported in part by the Japanese Science and Technology corporation for promoting Science and Technology in Japan, and in part by the Japan Aerospace Exploration Agency.

References

Ayers, J.K., Nguyen, L., Smith Jr., W.L. and Minnis, P., 1998, Calibration of geostationary satellite imager data for ARM using AVHRR. *Proceedings of 10th Conference on Atmospheric Radiation* (Long Beach, CA: American Meteorological Society).

Doelling, D.R., Nguyen, L., Smith Jr, W.L. and Minnis, P., 1998, Comparison of ARM GOES-derived broadband albedos with broadband data from ARM-UAV and ScaRaB. In *Proceedings of 10th Conference on Atmospheric Radiation* (Long Beach, CA: American Meteorological Society).

Fujii, H. and Koike, T., 2001, Development of a TRMM/TMI algorithm for precipitation in the Tibetan Plateau by considering effects of land surface emissivity. *Journal of the Meteorological Society of Japan*, **79**, pp. 475–483.

Horvath, A. and Davies, R., 2001, Simultaneous retrieval of cloud motion and height from polar-orbiter multi-angle measurements. *Geophysical Research Letters*, **28**, pp. 2915–2918.

Iguchi, T., Ohta, K., Oki, R., Sato, S., Shimizu, S., Kachi, M. and Higashiuwatoko, T., 2002, *Rain as Seen from Space, 4-year Observation from the Tropical Rainfall Measuring Mission Satellite*. Technical report, National Space Development Agency of Japan (Tokyo: Japan Advance Plan Co. Inc.), p. 75.

Jedlovec, G.J. and Laws, K., 2003, GOES cloud detection at the global hydrology and climate center. In *Proceedings of 12th Conference on Satellite Meteorology and Oceanography* (Long Beach, CA: American Meteorological Society).

Jensen, J.R., 2000, *Remote Sensing of the Environment: An Earth Resource Perspective* (Upper Saddle River, NJ: Prentice Hall).

Juarez, M.D., Kahn, B.H. and Fetzer, E.J., 2009, Cloud-type dependencies of MODIS and AMSR-E liquid water path differences. *Atmospheric Chemistry and Physics Discussions*, **9**, pp. 3367–3399.

Khaiyer, M.M., Rapp, A.D., Minnis, P., Doelling, D.R., Smith Jr, W.L., Nguyen, L., Nordeen, M.L. and Min, Q., 2002, Evaluation of a 5-year cloud and radiative property dataset derived from GOES-8 data over the southern Great Plains. In *Proceedings of 12th Atmospheric Radiation Measurement (ARM) Science Team Meeting* (Washington, DC: U.S. Department of Energy).

Kummerow, C., Hong, Y., Olson, W.S., Yang, S., Adler, R.F., McCollum, J., Ferraro, R., Petty, G., Shin, D. and Wilheit, T.T., 2001, The evolution of the Goddard Profiling Algorithm (GPROF) for rainfall estimation from passive microwave sensors. *Journal of Applied Meteorology*, **40**, pp. 1801–1820.

Li, L., Vivekanandan, J., Chan, C.H. and Tsang, L., 1997, Microwave radiometric technique to retrieve vapor, liquid and ice: part I – development of a neural network-based inversion method. *IEEE Transactions on Geoscience and Remote Sensing*, **35**, pp. 224–236.

Lillesand, T., Kiefer, R. and Chipman, J.W., 2004, *Remote Sensing and Image Interpretation* (Hoboken, NJ: John Wiley and Sons).

Liou, K.N. and Duff, A.D., 1979, Atmospheric liquid water content derived from parameterization of Nimbus 6 Scanning Microwave Spectrometer data. *Journal of Applied Metrology*, **18**, pp. 99–103.

Liu, G., 1998, A fast and accurate model for microwave radiance calculations. *Journal of the Meteorological Society of Japan*, **76**, pp. 335–343.

Minnis, P. and Harrison, E.F., 1984, Diurnal variability of regional cloud and clear-sky radiative parameters derived from GOES data; part III: November 1978 radiative parameters. *Journal of Climate and Applied Meteorology*, **23**, pp. 1032–1052.

Mirza, C.R., 2005, Development of a cloud microphysics data assimilation system over ocean for improved precipitation prediction by integrating satellite data. PhD thesis, University of Tokyo, Japan.

Nemoto, T., Koike, T. and Kitsuregawa, M., 2007, Data analysis system attached to the CEOP centralized data archive system. *Journal of the Meteorological Society of Japan*, **85A**, pp. 529–543.

Paloscia, S. and Pampaloni, P., 1988, Microwave polarization index for monitoring vegetation growth. *IEEE Transactions on Geoscience and Remote Sensing*, **26**, pp. 617–621.

Pfaff, T., 2003, Remote sensing of snowfall and cloud liquid water using ground based passive microwave radiometry. Master's thesis, University of Tokyo, Japan.

Saunders, R.W. and Kriebel, K.T., 1988, An improved method for detecting clear sky and cloudy radiances from AVHRR data. *International Journal of Remote Sensing*, **9**, pp. 123–150.

Ulaby, F.T., Moore, R.K. and Fung, A.K., 1981, *Microwave Remote Sensing: Fundamentals and Radiometry*, vol. 1 (Norwood, MA: Artech House).

Ulaby, F.T., Moore, R.K. and Fung, A.K., 1986, *Microwave Remote Sensing: From Theory to Applications*, vol. 3 (Norwood, MA: Artech House).

Vivekanandan, J., Li, L. and Tsang, L., 1997, Microwave radiometric technique to retrieve vapor, liquid and ice: part II – joint studies of radiometer and radar in winter clouds. *IEEE Transactions on Geoscience and Remote Sensing*, **35**, pp. 237–247.

Yang, K., Chen, Y.Y. and Qin, J., 2009, Some practical notes on the land surface modeling in the Tibetan Plateau. *Hydrology and Earth System Sciences Discussions*, **6**, pp. 1291–1320.

Yang, K., Koike, T., Ye, B. and Bastidas, L., 2005, Inverse analysis of the role of soil vertical heterogeneity in controlling surface soil state and energy partition. *Journal of Geophysical Research*, **110**, D08101, doi:10.1029/2004JD005500.

Yang, K., Watanabe, T., Koike, T., Li, X., Fujii, H., Tamagawa, K., Ma, Y. and Ishikawa, H., 2007, Auto-calibration system developed to assimilate AMSR-E data into a land surface model for estimating soil moisture and the surface energy budget. *Journal of the Meteorological Society of Japan*, **85A**, pp. 229–242.